Magnetic Fields in the Formation of Massive Stars

Josep M. Girart,[1]* Maria T. Beltrán,[2]† Qizhou Zhang,[3] Ramprasad Rao,[4] Robert Estalella[2]

Massive stars play a crucial role in the production of heavy elements and in the evolution of the interstellar medium, yet how they form is still a matter of debate. We report high-angular-resolution submillimeter observations toward the massive hot molecular core (HMC) in the high-mass star-forming region G31.41+0.31. We find that the evolution of the gravitational collapse of the HMC is controlled by the magnetic field. The HMC is simultaneously contracting and rotating, and the magnetic field lines threading the HMC are deformed along its major axis, acquiring an hourglass shape. The magnetic energy dominates over the centrifugal and turbulence energies, and there is evidence of magnetic braking in the contracting core.

Stars more massive than 8 $M_\odot$ (where $M_\odot$ is the mass of the Sun) account for only 1% of the stellar population in our Galaxy. Nevertheless they dominate the appearance and evolution of its interstellar medium and are responsible for the production of heavy elements.

The formation of massive stars is not completely understood. Stars form when dense molecular clouds collapse as a result of gravity. But as the mass of a young star reaches 8 $M_\odot$, its own radiation can exert enough outward pressure to halt infall, inhibiting further stellar growth (*1*). The presence of a flattened accretion disk surrounding the protostar (*2*) can alleviate this inhibition by shielding the infalling material from stellar radiation and by creating a lower density section along the rotation axis of the disk and a molecular outflow, which helps by channeling the radiation out, allowing the formation of stars more massive than 40 $M_\odot$ (*3*–*5*). Massive stars may also form through mergers of smaller stars (*6*).

The scenario whereby massive stars form through disk-assisted accretion resembles the way stars like the Sun form. Both processes involve accretion through a flattened disk and molecular outflows. The magnetic field is thought to play an important role in the formation of Sun-like stars by shaping cloud collapse, removing excess angular momentum, and thus allowing continuous accretion (*7*–*9*), even in the case of an originally weak magnetic field (*10*). High-angular-resolution polarimetric observations of the low-mass protostellar system NGC 1333 IRAS 4A (IRAS 4A) showed a magnetic field with a clear hourglass morphology at scales of a few hundred astronomical units (AU) around the collapsing molecular core surrounding the protostars (*11*), a configuration that was shown to be consistent with theoretical models for the formation of solar-type stars, where well-ordered, large-scale, rather than turbulent, magnetic fields control the evolution and collapse of the molecular cores from which stars form (*12*).

We investigated the hot molecular core (HMC) in G31.41+0.31 (G31.41), a massive star-forming region [~500 to 1500 $M_\odot$ (*13*, *14*)] located 7900 parsecs (pc) away (*15*). G31.41 has a luminosity

[1]Institut de Ciències de l'Espai [Consejo Superior de Investigaciones Científicas (CSIC)–Institut d'Estudis de Catalunya (IEEC)], Campus Universitat Autònoma de Barcelona (UAB)–Facultat de Ciències, Torre C5 - parell 2[a], 08193 Bellaterra, Catalunya, Spain. [2]Departament d'Astronomia i Meteorologia (IEEC-UB). Institut de Ciencies del Cosmos y Unitat Associada a CSIC, Universitat de Barcelona, Martí i Franquès 1, 08028 Barcelona, Catalunya, Spain. [3]Harvard-Smithsonian Center for Astrophysics, 60 Garden Street, Cambridge, MA 02138, USA. [4]Academia Sinica, Institute of Astronomy and Astrophysics, 645 North Aohoku Place, Hilo, HI 96720, USA.

*To whom correspondence should be addressed. E-mail: girart@ieec.cat

†Present address: Osservatorio Astrofisico di Arcetri, Largo Enrico Fermi 5, 50125 Firenze, Italy.

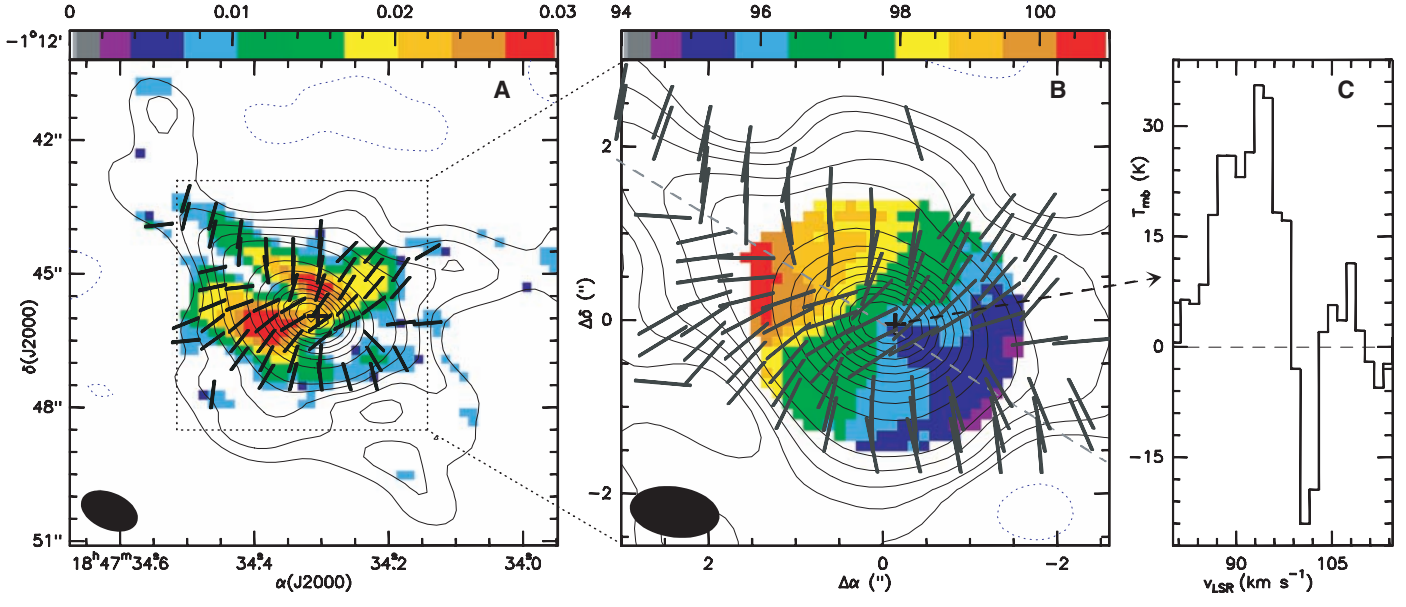

Fig. 1. (**A**) Contour map of the 879-μm dust emission superposed on the color image of the polarized flux intensity in units of Jy per beam. Black thick bars indicate the position angle of the magnetic field. These maps were obtained by using a natural weighting to the visibility data, which yielded to a full width at half maximum synthesized beam of 1.34″ × 0.83″ with a position angle of 67° (shown in the bottom left corner). Contour levels are 0.8, 1.5, 2.5, 4, 6, 16, 26, 36…96% of the peak intensity, 9.13 Jy per beam. (**B**) Contour map of the 879 μm dust emission superposed on the color image of the flux weighted velocity map of the CH_3OH 14_7-15_6 A. Black thick bars indicate the direction of the magnetic field. These maps were obtained by using a robust weighting of 0 to the visibility data, which yielded to a full width at half maximum synthesized beam of 1.04″ × 0.59″ with a position angle of 82° (shown in the bottom left corner). Contour levels are the same as in the previous panel, with a peak intensity of 6.55 Jy per beam. (**C**) Spectrum of the $C^{34}S$ 7-6 line at the position of the dust emission peak. The continuum has been subtracted from the line emission (this is valid for all the molecular line data presented here).

of 3×10^5 $L_\odot$ (where $L_\odot$ is the luminosity of the Sun), suggesting that the core's center harbors O-type hydrogen-burning stars (*14*, *15*). It is associated with very weak free-free emission (*16*), implying that an ultracompact HII region has not yet developed and therefore that the embedded young stellar objects are in a very early stage of their evolution. High-angular-resolution observations of methyl cyanide toward the HMC reveal a massive toroid (*13*, *17*) rotating about the axis of a bipolar outflow (*18*), the direction of which is controversial (*16*). The mass of the toroid is much larger than the dynamical mass required for equilibrium (~87 $M_\odot$) (*13*), which suggests that the toroid may be gravitationally unstable and undergoing collapse, unless a strong (20 to 40 mG) magnetic field is present. The physical properties of the HMC have been modeled recently, with an infall radius smaller than $\sim 2 \times 10^4$ AU and a high accretion rate of 3×10^{-3} $M_\odot$ year^{-1} (*14*).

We observed G31.41 at 879 μm with use of the Submillimeter Array (SMA) (*19*) in its compact and extended configurations (which provides an angular resolution slightly below 1 arc sec: see Fig. 1) and with use of the SMA polarimetry system (*20*). The continuum emission, which traces the dust in the HMC, is resolved in a slightly elongated compact component with a size of 1.16″ by 0.93″ (8100 AU by 6500 AU) and a position angle (PA) of 56°, surrounded by a weaker component extending to the northeast and reaching an ultracompact HII region located 5″ northeast of the HMC (*15*). The total flux measured in our 879-μm observations is 21.2 ± 1.0 janskys (Jy, 1 Jy = 10^{-26} W m^{-2} Hz^{-1}) over an area of 15.9 square arc sec, where there is adequate sensitivity to measure the polarization. For an optically thin emission, a temperature of 164 K (*15*), a gas-to-dust ratio of 100, and a dust opacity of 1.9 cm^2 g^{-1} (*21*), the total mass traced by the dust is 577 $d_{7.9}$ $M_\odot$ [$d_{7.9} \equiv (d/7.9\ \text{kpc})$, where d is the adopted distance to the G31.41 cloud], in the range of previous estimations (*13*, *14*). We can estimate the averaged column and volume density of the region traced by the dust: $\langle N(H_2) \rangle = M/(A\mu_m)$ and $\langle n(H_2) \rangle = M/(V\mu_m)$, where M is the dust mass, μ_m is the average mass per particle, A is the area of the dust emission, and $V = (4/3)\pi^{-1/2}A^{3/2}$ is the volume. For a helium-to-hydrogen mass ratio of 30%, the mean column density is $\langle N(H_2) \rangle = 3.5 \times 10^{24}$ cm^{-2}, and the mean volume density is $\langle n(H_2) \rangle = 3.1 \times 10^6 d_{7.9}^{-1}$ cm^{-3}.

We detected linearly polarized dust emission in the HMC, mainly along the major axis of the dust emission (color scale in Fig. 1A), with a maximum polarized flux of 30 mJy per beam. At the position of the maximum polarized flux, the polarization fraction is at a 4% level. The position angle of the dust polarization allows us to examine the magnetic field. Thus, at the spatial scale of the SMA angular resolution, ~6000 AU, the magnetic field lines are deformed along the major axis of the HMC (Fig. 1, A and B), providing evidence of an hourglass magnetic field configuration in a high-mass star-forming region. An hourglass configuration was also found in the OMC-1 (*22*), but it was at much larger scales (~0.5 pc) and in a more-complex and -evolved high-mass star-forming region.

The 4 GHz of bandwidth available for the SMA allowed us to detect a large number of spectral lines. The myriad of lines is dominated by CH_3OH, with more than 30 lines, but also by $HCOOCH_3$, CH_3OCH_3, and SO_2. Many of the lines show a similar morphological and kinematical pattern in the HMC. There is a broad range of excitation conditions among the molecular lines detected, with upper energy levels going from a few tens up to more than 1000 K. In general, the emission is more compact for the lines with a higher excitation energy level, showing a velocity gradient along the major axis (Fig. 1B), which is suggestive of rotation, as previously found for CH_3CN (*13*). One of the lowest excitation lines, $C^{34}S$ 7-6, shows a clear inverse P-Cygni profile in its spectrum (Fig. 1C). The emission feature peaks at about 93.5 km s^{-1} and the absorption feature at about 100.5 km s^{-1}, whereas the cloud velocity, V_{LSR}, is ≈97.4 km s^{-1} (*14*). The colder molecular gas from the circumstellar envelope absorbs the bright continuum emission. The absorption at positive velocities (i.e., redshifted because of the Doppler effect) relative to the cloud velocity and the presence of the blueshifted emission imply that the circumstellar envelope at scales of a few thousand AUs is infalling. The infall velocity, which has been estimated as $|V_{LSR} - V_{redshifted}|$, is ~3.1 km s^{-1}.

We proceeded, similarly to (*11*), to derive the magnetic field properties by first fitting its morphology with a family of exponential functions. We find that the center of symmetry of the magnetic field coincides within the measured uncertainty, ~0.2", with the center of the core (i.e., the position of the dust emission peak). The position angle of the magnetic field axis, ≈–27°, is almost perpendicular to the major axis of the envelope (Fig. 2). There are some discrepancies southwest of the center where the measured field directions suggest a small tilt of the major axis westward of the center. The observed dispersion in the residuals (fig. S1), $\delta\theta_{obs}$, is 13.6 ± 1.0°. Because the measurement uncertainty of the polarization angle (σ_θ) is 9.5 ± 3.3°, the intrinsic dispersion, $\delta\theta_{int} = (\delta\theta_{obs}^2 - \sigma_\theta^2)^{1/2}$, is $\delta\theta_{int}$ = 9.8 ± 3.5°. The magnetic field strength can be estimated from the dispersion in polarization angles (which is a consequence of the perturbation by Alfvén waves or turbulence in the field lines). With use of the value of the volume density derived from our data, $n(H_2) = 3.1 \times 10^6$ cm^{-3}, and a turbulent velocity dispersion of $\delta v_{los} \approx 2.7$ km s^{-1}, the expected value from the Osorio *et al.* modeling (*14*) at the scale of $\approx 1.5 \times 10^4$ AU, which is the scale of the observed polarized emission—we calculated

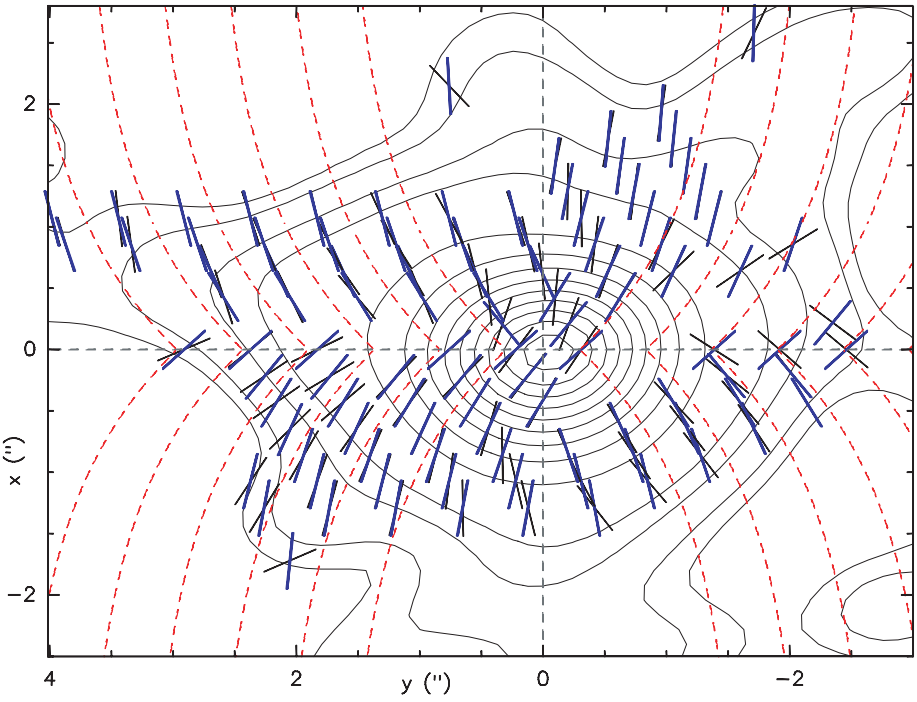

Fig. 2. Magnetic field directions superposed on the contour map of the dust emission. The map has been rotated by 27° to the east with respect to the one shown in Fig. 1. Contour levels are at 0.9, 1.4, 3, 5, 15, … 95% of the intensity peak. The black bars show the vectors of the measured magnetic fields. The blue bars correspond to the best fit to the magnetic field lines assuming an exponential form of $y = y_0 - C_1\exp(-C_2 x)$, where the x is the distance from the center of the symmetry along the magnetic field axis. The fit was done by using a χ^2 analysis with the following free parameters: $\langle_0$ and $_0$, the center of symmetry; $\langle_{PA}$, the position angle of the field axis, C_1 and C_2. The best fit is obtained when $\langle_{PA} = -27° \pm 1°$, $\langle_0(J2000) = 18^h47^m34.31^s \pm 0.02^s$, $_0(J2000) = -1°12'46.0'' \pm 0.2''$, $C_1 = 0.8 \pm 0.2$, and $C_2 = 1.4 \pm 0.4$. The red dashed lines show the exponential shape of the best-fit field.

the magnetic field strength in the plane of the sky to be $B_{pos} \approx 9.7 d_{7.9}^{-1/2}$ mG. This value is a factor of ~2 higher that an earlier value derived by the Osorio *et al*. (*14*) assuming equipartition between the magnetic and turbulent energy. The magnetic field strength in G31.41 is also higher than those in other massive star-forming cores (*23*, *24*). The derived value of the magnetic field strength implies an Alfvenic velocity of $v_A = \sqrt{B/(4\pi\rho)} =$ 7.9 km s^{-1}, which is larger than the infall velocity, so the collapse is sub-Alfvenic. The key parameter that determines whether magnetic fields provide support against gravitational collapse is the mass–to–magnetic flux ratio. With use of the standard formula (*25*), we find that the mass–to–magnetic flux ratio is $\approx 2.7 d_{7.9}^{1/2}$ times the critical value for collapse. The ratio of the turbulent to magnetic energy, $\beta_{turb} = 3(\delta v_{los}/v_A)^2 = 3.64 \times 10^{-3} (\delta\theta_{int}/^\circ)^2$, is $\beta_{turb} = 0.35^{+0.29}_{-0.20}$, indicating that the magnetic energy dominates over the turbulent energy. This ratio is a lower limit, and the mass-to-flux ratio is an upper limit because what is measured is the component on the plane of the sky of the magnetic field strength. However, the deprojected values are likely not too different because, first, the clear hourglass morphology suggests that the HMC is not close from the pole-on configuration and, second, the size of the major and minor axes are similar, so it is reasonable to use the estimated column density to derive the mass–to–magnetic flux ratio.

The mass accretion rate can be estimated from the infall velocity derived from the inverse P-Cygni profile. Although the associated infall radius is uncertain, we have chosen a lower limit of 4080 AU, which corresponds to the source radius obtained from Gaussian deconvolution of the continuum image, and an upper limit of 12,640 AU, which corresponds to the radius of the emission at 5% of the peak emission, which includes most of the dust emission. Following Beltrán *et al*. (*26*), the mass accretion rate onto the star ($4\pi R^2 m H_2 n V_{infall}$) inside a solid angle Ω is $M_{acc} = \Omega/(4\pi)(3 \times 10^{-3}$ to $3 \times 10^{-2}) M_\odot$ year^{-1}, which is in agreement with the estimate from modeling G31.41 (*14*). Such a high value of the infall rate has also been estimated for other O-type (proto)stars (*26*–*28*), supporting the nonspherical accretion scenario for the formation of massive stars, which is expected in the presence of a substantial magnetic field, as observed here.

Here on, we study the kinematical behavior resulting from the velocity gradient along the major axis of the HMC, which is indicative of rotation (this is supported by the fact that this velocity gradient is perpendicular to the hourglass magnetic field shape). To avoid chemical effects that could affect the interpretation, we used only methanol transitions, which is the most populated species within the observed bandwidth. Of these lines, we selected only those with upper excitation energy levels that range from 60 to 1020 K and appear clean of interlopers (Fig. 3). The lower excitation lines (top graphs of Fig. 3) show a relative minimum at redshifted velocities toward the center, which is indicative of infall, as found more clearly in the even lower excitation $C^{34}S$ line. The position-velocity maps reveal a smaller velocity gradient, that is, a smaller rotation velocity, in the more spatially compact lines (typically the higher excitation ones) (Fig. 4). For a collapsing core with angular momentum conservation and with a very weak magnetic field, the rotation velocity is expected to be inversely proportional to the radius (*10*). This is the opposite of what is observed in the HMC, in which the rotation velocity decreases for decreasing radius, indicating that the angular momentum is not conserved during the collapse. Given the hourglass magnetic field morphology in the HMC, this spin-down in the HMC suggests magnetic braking, a process proposed to remove the excess of angular momentum. Theoretical models of magnetic braking predict a spin-down qualitatively in agreement with what is shown in Fig. 4 (*7*, *10*). Depending on the value of the rotation velocity and the magnetic field, the evolution of a collapsing core is regulated either by the centrifugal forces or by the magnetic forces (*29*). If the measured (ω/*B*) value is larger than

$$\left(\frac{\omega_{st}}{B}\right)_{crit} = 1.69 \times 10^{-7} \times \left(\frac{c_s}{0.19 \mathrm{km/s}}\right)^{-1} \mathrm{year}^{-1}\,\mu\mathrm{G}^{-1},$$

where c_s is the sound speed and ω is the angular velocity, the centrifugal forces dominate the dynamics. Otherwise the magnetic forces regulate the dynamics. For c_s=0.93 km s^{-1}, we found that the measured ratio, 6.6×10^{-9} year^{-1} μG^{-1}, is smaller than the critical value, 3.5×10^{-8} year^{-1} μG^{-1}. Thus, the magnetic field dominates energetically (with respect to centrifugal and turbulence forces) the dynamics of the collapse.

The HMC in G31.41 is much larger (by a factor of 20) and more massive (by a factor of 200) and luminous (by five orders of magnitudes) than the Sun-like IRAS 4A. However, both sources show an inverse P-Cygni profile, indicative of

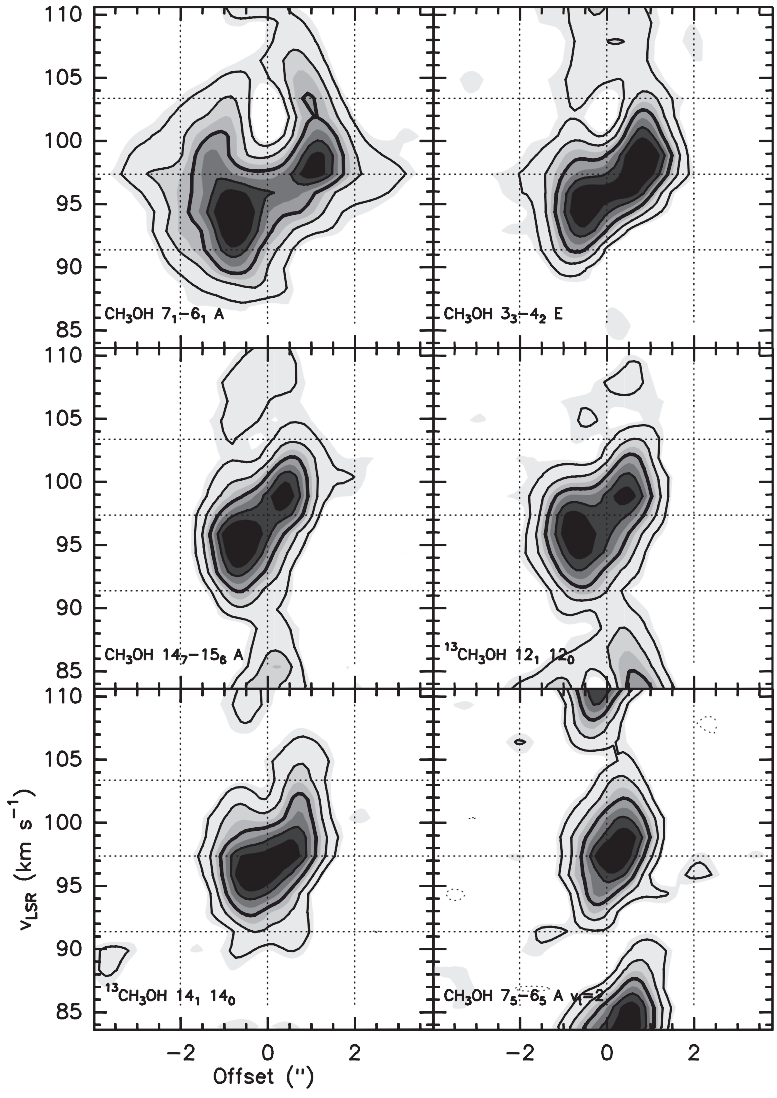

Fig. 3. Position-velocity cuts along a position angle of 65° (close to the major axis of the HMC) for six methanol lines (their transitions are labeled in the lower left part of each graph). The zero offset position is located at the position of the Very Large Array 7-mm source A (*16*). Contour levels are the 15, 30, 50 (thicker contour), 70, and 90% of the peak intensity of each transition. The central horizontal dotted line shows the cloud velocity.

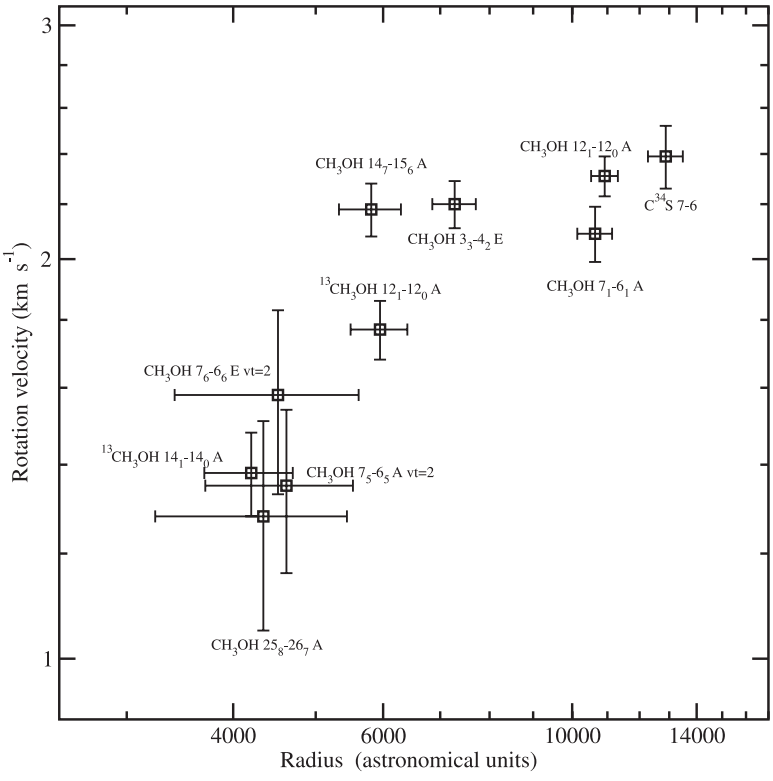

Fig. 4. The distribution of the rotation velocity as a function of the radius. These values were derived from the integrated intensity and the intensity weighted mean velocity maps at the position where the dust major axis intersects the half maximum contour level from the integrated emission (the velocity gradient is observed along the major axis; see Fig. 1).

infall motions (*30*), and have similar magnetic field properties (a hourglass configuration approximately along the major axis and a similar mass-to-flux ratio). The energetic relations do not differ too much, either: Both cores are collapsing because gravity has overcome pressure forces, but the collapsing dynamics are controlled by the magnetic energy rather than by turbulence. This similarity suggests that the role of the magnetic field in the early stages of the formation of high- and low-mass stars may not be too different. However, once the massive stars turn on an ultracompact HII, the feedback from the massive stars (radiation and ionization pressure, turbulence, and outflows) becomes energetically more important than the magnetic fields (*31*).

References and Notes

1. M. G. Wolfire, J. P. Cassinelli, *Astrophys. J.* **319**, 850 (1987).
2. T. Nakano, *Astrophys. J.* **345**, 464 (1989).
3. H. W. Yorke, C. Sonnhalter, *Astrophys. J.* **569**, 846 (2002).
4. M. R. Krumholz, C. F. McKee, R. I. Klein, *Astrophys. J.* **618**, L33 (2005).
5. M. R. Krumholz, R. I. Klein, C. F. McKee, S. S. R. Offner, A. J. Cunningham, *Science* **323**, 754 (2009); published online 15 January 2009 (10.1126/science.1165857).
6. I. A. Bonnell, M. R. Bate, *Mon. Not. R. Astron. Soc.* **362**, 915 (2005).
7. S. Basu, T. Ch. Mouschovias, *Astrophys. J.* **432**, 720 (1994).
8. A. P. Boss, *Astrophys. J.* **658**, 1136 (2007).
9. D. Galli, S. Lizano, F. H. Shu, A. Allen, *Astrophys. J.* **647**, 374 (2006).
10. R. Mellon, Z.-Y. Li, *Astrophys. J.* **681**, 1356 (2008).
11. J. M. Girart, R. Rao, D. P. Marrone, *Science* **313**, 812 (2006).
12. J. Gonçalves, D. Galli, J. M. Girart, *Astron. Astrophys.* **490**, L39 (2008).
13. M. T. Beltrán *et al.*, *Astrophys. J.* **601**, L187 (2004).
14. M. Osorio, G. Anglada, S. Lizano, P. D'Alessio, *Astrophys. J.* **694**, 29 (2009).
15. R. Cesaroni, E. Churchwell, P. Hofner, C. M. Walmsley, S. Kurtz, *Astron. Astrophys.* **288**, 903 (1994).
16. E. Araya, P. Hofner, S. Kurtz, L. Olmi, H. Linz, *Astrophys. J.* **675**, 420 (2008).
17. M. T. Beltrán *et al.*, *Astron. Astrophys.* **435**, 901 (2005).
18. L. Olmi, R. Cesaroni, C. M. Walmsley, *Astron. Astrophys.* **307**, 599 (1996).
19. P. T. P. Ho, J. M. Moran, K. Y. Lo, *Astrophys. J.* **616**, L1 (2004).
20. D. P. Marrone, J. M. Moran, J.-H. Zhao, R. Rao, *Astrophys. J.* **640**, 308 (2006).
21. V. Ossenkopf, T. Henning, *Astron. Astrophys.* **291**, 943 (1994).
22. D. A. Schleuning, *Astrophys. J.* **493**, 811 (1998).
23. S.-P. Lai, R. M. Crutcher, J. M. Girart, R. Rao, *Astrophys. J.* **561**, 864 (2001).
24. P. Cortes, R. M. Crutcher, *Astrophys. J.* **639**, 965 (2006).
25. T. C. Mouschovias, L. Spitzer Jr., *Astrophys. J.* **210**, 326 (1976).
26. M. T. Beltrán *et al.*, *Nature* **443**, 427 (2006).
27. E. R. Keto, P. T. P. Ho, A. D. Haschick, *Astrophys. J.* **318**, 712 (1987).
28. L. A. Zapata *et al.*, *Astron. Astrophys.* **479**, L25 (2008).
29. M. N. Machida, T. Matsumoto, K. Tomisaka, T. Hanawa, *Mon. Not. R. Astron. Soc.* **362**, 369 (2005).
30. J. Di Francesco, P. C. Myers, D. J. Wilner, N. Ohashi, D. Mardones, *Astrophys. J.* **562**, 770 (2001).
31. Y. W. Tang *et al.*, *Astrophys. J.* **695**, 1399 (2009).

32. The Submillimeter Array is a joint project between the Smithsonian Astrophysical Observatory and the Academia Sinica Institute of Astronomy and Astrophysics and is funded by the Smithsonian Institution and the Academia Sinica. We thank D. Galli, R. R. Cesaroni, and J. M. Torrelles for helpful comments. J.M.G., M.T.B., and R.E. acknowledge Ministerio de Ciencia e Innovación (Spain) for support through grants AYA2005-08523-C03 and AYA2008-06189-C03. J.M.G. also acknowledges support from Agència de Gestió d'Ajuts Universitaris i de Recerca 2005-SGR00489 grant.

Supporting Online Material

www.sciencemag.org/cgi/content/full/324/5933/1408/DC1
Fig. S1

3 February 2009; accepted 30 April 2009
10.1126/science.1171807

A Radio Pulsar/X-ray Binary Link

Anne M. Archibald,[1]* Ingrid H. Stairs,[2,3,4] Scott M. Ransom,[5] Victoria M. Kaspi,[1] Vladislav I. Kondratiev,[6,5,7] Duncan R. Lorimer,[6,8] Maura A. McLaughlin,[6,8] Jason Boyles,[6,8] Jason W. T. Hessels,[9,10] Ryan Lynch,[11] Joeri van Leeuwen,[9,10] Mallory S. E. Roberts,[12] Frederick Jenet,[13] David J. Champion,[3] Rachel Rosen,[8] Brad N. Barlow,[14] Bart H. Dunlap,[14] Ronald A. Remillard[15]

Radio pulsars with millisecond spin periods are thought to have been spun up by the transfer of matter and angular momentum from a low-mass companion star during an x-ray–emitting phase. The spin periods of the neutron stars in several such low-mass x-ray binary (LMXB) systems have been shown to be in the millisecond regime, but no radio pulsations have been detected. Here we report on detection and follow-up observations of a nearby radio millisecond pulsar (MSP) in a circular binary orbit with an optically identified companion star. Optical observations indicate that an accretion disk was present in this system within the past decade. Our optical data show no evidence that one exists today, suggesting that the radio MSP has turned on after a recent LMXB phase.

The fastest-spinning radio millisecond pulsars (MSPs) are thought to be formed in systems containing a neutron star (NS) and a low-mass [$\lesssim$1 solar mass ($M_\odot$)] companion star (*1*). Mass transfer occurs when matter overflows the companion's Roche lobe (*2*), forms an accretion disk around the NS, and eventually falls onto its surface, producing bright x-ray emission (*1*, *3*).

Radio emission that would otherwise be produced by a rapidly rotating magnetic NS is thought to be quenched during active accretion by the presence of ionized material within the pulsar's light cylinder. However, at a sufficiently low accretion rate, infalling material may be halted outside the light cylinder by magnetic pressure, presumably allowing the MSP's radio emission to turn on. At this point, the MSP's electromagnetic emission and particle wind should irradiate the disk and companion, driving mass out of the system. This activation as a radio pulsar, a possible

Science

Magnetic Fields in the Formation of Massive Stars

Josep M. Girart, Maria T. Beltrán, Qizhou Zhang, Ramprasad Rao, and Robert Estalella

Science, 324 (5933), • DOI: 10.1126/science.1171807

Stellar Hourglass Figure

Star-forming clouds are thought to be supported against gravity by ordered interstellar magnetic fields, which are strong enough to slow gravitation collapse but too weak to prevent it. Girart *et al.* (p. 1408) measured polarized radio waves from dust particles around a forming massive star, which reveal an hourglass shape. The data imply that a magnetic field strength dominates over turbulence—the telltale signs of magnetically controlled star formation. These conditions mimic those found in low-mass star-forming regions, suggesting that the magnetic field plays an important role in star formation, irrespective of differences in mass.

Science (ISSN 1095-9203) is published by the American Association for the Advancement of Science. 1200 New York Avenue NW, Washington, DC 20005. The title *Science* is a registered trademark of AAAS.